Propagation of CaMKII translocation waves in heterogeneous spiny dendrites

Paul C. Bressloff

Journal of Mathematical Biology

ISSN 0303-6812
Volume 66
Number 7

J. Math. Biol. (2013) 66:1499-1525
DOI 10.1007/s00285-012-0542-9

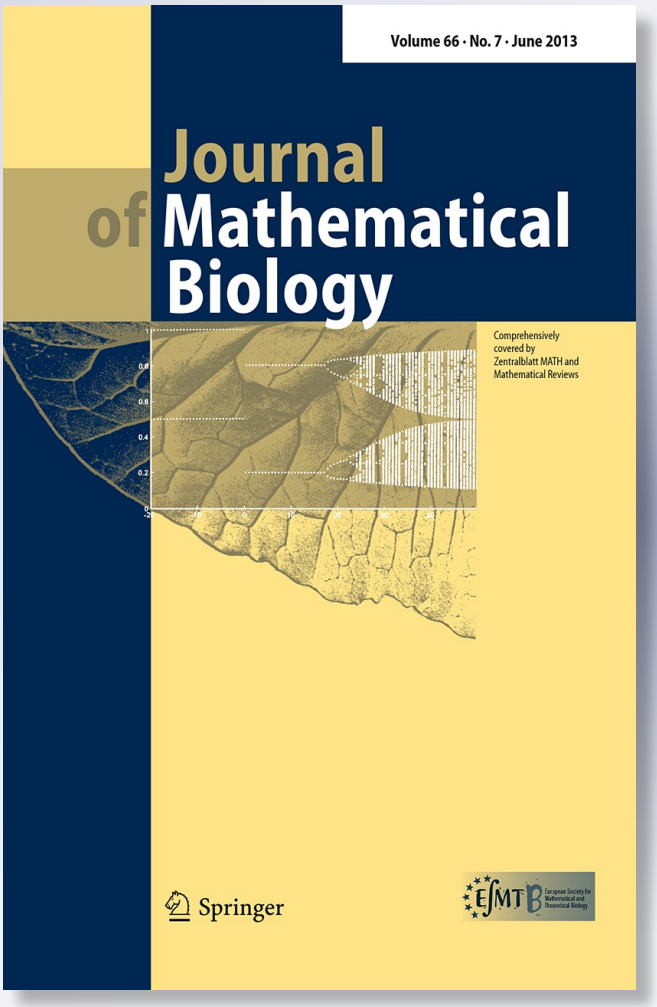

Springer

J. Math. Biol. (2013) 66:1499–1525
DOI 10.1007/s00285-012-0542-9

Mathematical Biology

Propagation of CaMKII translocation waves in heterogeneous spiny dendrites

Paul C. Bressloff

Received: 26 November 2011 / Revised: 18 April 2012 / Published online: 16 May 2012

Abstract CaMKII (Ca^{2+}-calmodulin-dependent protein kinase II) is a key regulator of glutamatergic synapses and plays an essential role in many forms of synaptic plasticity. It has recently been observed experimentally that stimulating a local region of dendrite not only induces the local translocation of CaMKII from the dendritic shaft to synaptic targets within spines, but also initiates a wave of CaMKII translocation that spreads distally through the dendrite with an average speed of order 1μm/s. We have previously developed a simple reaction–diffusion model of CaMKII translocation waves that can account for the observed wavespeed and predicts wave propagation failure if the density of spines is too high. A major simplification of our previous model was to treat the distribution of spines as spatially uniform. However, there are at least two sources of heterogeneity in the spine distribution that occur on two different spatial scales. First, spines are discrete entities that are joined to a dendritic branch via a thin spine neck of submicron radius, resulting in spatial variations in spine density at the micron level. The second source of heterogeneity occurs on a much longer length scale and reflects the experimental observation that there is a slow proximal to distal variation in the density of spines. In this paper, we analyze how both sources of heterogeneity modulate the speed of CaMKII translocation waves along a spiny dendrite. We adapt methods from the study of the spread of biological invasions in heterogeneous environments, including homogenization theory of pulsating fronts and Hamilton–Jacobi dynamics of sharp interfaces.

Keywords CaMKII · Pulsating fronts · Homogenization · Spiny dendrites · Hamilton–Jacobi dynamics · Heterosynaptic plasticity

Mathematics Subject Classification 92C20 · 35C07

P. C. Bressloff (✉)
Department of Mathematics, University of Utah, Salt Lake City, UT 84112, USA
e-mail: bressloff@math.utah.edu

1 Introduction

Reaction–diffusion equations based on the Fisher–Kolmogorov et al. (F-KPP) model and its generalizations have been used extensively to describe the spatial spread of invading species including plants, insects, diseases and genes (Fisher 1937; Kolmogorov et al. 1937; Murray 1989; Holmes et al. 1994; Shigesada and Kawasaki 1997; Cantrell and Cosner 2003; Volpert and Petrovskii 2009). Although such models were originally formulated under the assumption that the environment is homogeneous, there is a growing interest in taking into account spatial heterogeneities. This reflects the fact that there is often a patch-like mosaic of heterogeneous habitats (forests, plains etc.), which are fragmented by natural or artificial barriers (rivers, roads, cultivated fields etc.). In recent years, a number of analytical and numerical methods have been developed to study propagating invasive fronts in periodic and random media (Gartner and Freidlin 1979; Shigesada et al. 1986; Shigesada and Kawasaki 1997; Xin 2000; Weinberger 2002; Kinezaki et al. 2003; Cantrell and Cosner 2003; Berestycki et al. 2005; El Smaily et al. 2009). Heterogeneity is often incorporated by assuming that the diffusion coefficient and the growth rate of a population are periodically varying functions of space. One of the simplest examples of a single population model in a periodic environment was proposed by Shigesada et al. (Shigesada et al. 1986; Shigesada and Kawasaki 1997), in which two different homogeneous patches are arranged alternately in one-dimensional space so that the diffusion coefficient and the growth rate are given by periodic step functions. The authors showed how an invading population starting from a localized perturbation evolves to a traveling periodic wave in the form of a pulsating front. By linearizing around the leading edge of the wave, they also showed how the minimal wavespeed of the pulsating front could be estimated by finding solutions of a corresponding Hill equation (Shigesada et al. 1986). An alternative method for analyzing fronts in heterogeneous media, which is applicable to slowly modulated environments, was originally developed by Freidlin (Gartner and Freidlin 1979; Freidlin 1985, 1986) using large deviation theory, and subsequently reformulated in terms of PDEs by Evans and Sougandis (1989). The basic idea is to rescale space and time so that the front becomes a sharp interface whose location can be determined by solving a corresponding Hamilton–Jacobi equation.

In this paper we extend the theory of wave propagation in heterogeneous environments to a problem in cellular neurophysiology, namely, the translocation of Ca^{2+}–calmodulin-dependent protein kinase II (CaMKII) in spiny dendrites. There is now considerable experimental evidence suggesting that CaMKII is one of the most important signaling molecules involved in the induction of synaptic plasticity (Hudmon and Schulman 2002; Lisman et al. 2002). There are a number of reasons for this. First, CaMKII is found to be abundant at postsynaptic sites where it can detect changes in the local levels of Ca^{2+} entering the synapse following plasticity-inducing stimuli, via binding of CaMKII to Ca^{2+}/CaM. Activated CaMKII then phosphorylates substrates responsible for the expression of synaptic plasticity, namely, the number and the conductivity of synaptic AMPA receptors (Fukunaga et al. 1995; Mammen et al. 1997; Barria et al. 1997a; Derkach et al. 1999; Lee et al. 2009). Second, once activated, CaMKII can transition into a Ca^{2+}/CaM-independent, hyper-activated state via the autophosphorylation of neighboring enzymatic subunits (Hanson et al. 1994;

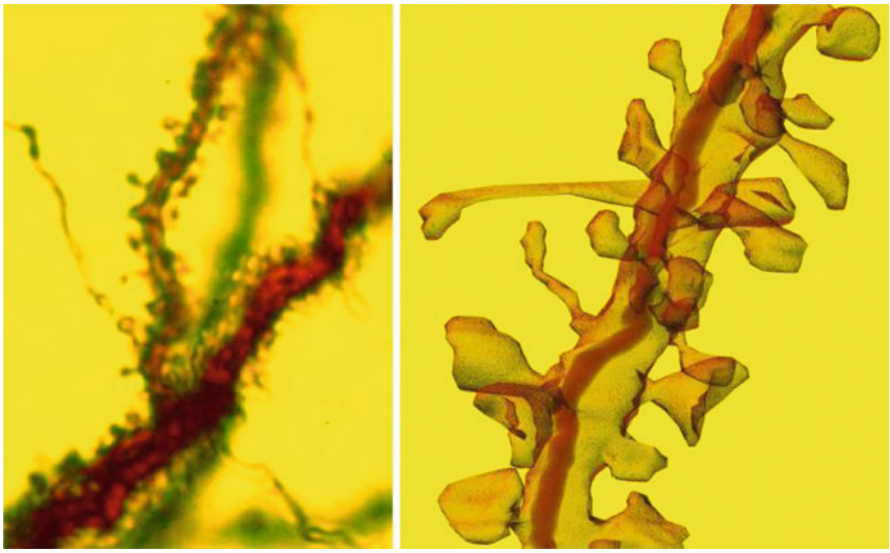

Fig. 1 An example of a piece of spine studded dendritic tissue (from rat hippocampal region CA1 stratum radiatum). Magnified view on *right-hand side* shows a dendrite ∼5 μm in length. Taken with permission from SynapseWeb, Kristen M. Harris, PI (http://synapses.clm.utexas.edu/)

Rich and Schulman 1998), and thus continue to phosphorylate its substrates even after the plasticity-inducing Ca^{2+} signal has ended (Saitoh and Schwartz 1985; Miller and Kenney 1986; Lou et al. 1986; Yang and Schulman 1999). Third, suppression of CaMKII using chemical antagonists blocks all known forms of NMDA receptor-dependent long-term potentiation (LTP) (Malinow et al. 1989; Fukunaga et al. 1993; Pettit et al. 1994; Lledo 1995; Barria et al. 1997b; Otmakhov et al. 1997; Malenka and Bear 2004).

Most excitatory synapses in the brain are located within dendritic spines, which are small, sub-micrometer membranous extrusions that protrude from a neuron's dendrite (Yuste 2010). Typically spines have a bulbous head which is connected to the parent dendrite through a thin spine neck, see Fig. 1. Confinement of CaMKII within spines arises from the geometry of the spine and through interactions with protein receptors and cytoskeletal elements within the postsynaptic density (PSD), which is the protein–rich region at the tip of the spine head. Global stimulation of NMDA receptors has previously been shown to result in the translocation of CaMKII from the dendritic shaft into spines (Strack et al. 1997; Shen and Meyer 1999; Shen et al. 2000; Bayer 2006). There are two main isoforms of CaMKII, known as CaMKIIα and CaMKIIβ. In its inactive state CaMKIIα tends to be located in the cytosol, whereas CaMKIIβ is weakly actin bound (Shen et al. 1998). Following Ca^{2+}-induced activation, CaMKII accumulates at post-synaptic sites through binding to NMDA receptors (Gardoni 1998; Leonard et al. 1999; Bayer et al. 2001). If the calcium signal is relatively weak then this binding is rapidly reversible, whereas for stronger stimulation the synaptic accumulation of CaMKII can persist for several minutes due to autophosphorylation. Recently, Rose et al. used a local rather than global signal to induce

translocation of CaMKII into spines, by stimulating a 30 μm wide region of dendrite with a 15 ms puff of 100 μM glutamate and 10 μM glycine. Interestingly, this initiated a wave of CaMKII translocation that spread toward the distal end of the dendrite with an average speed of ∼1 μm/s. They also observed that the wave was preceded by a much faster Ca^{2+} spike mediated by L-type Ca^{2+} channels, which they hypothesized could provide a mechanism for priming CaMKII outside the stimulus region for diffusion-based activation. They found translocation waves in both excitatory pyramidal neurons and inhibitory interneurons for both the α and β isoforms of CaMKII. Moreover, the CaMKII translocation wave was associated with an increase in AMPA receptor numbers at both stimulated and non-stimulated synapses (Rose et al. 2009). This suggests that it could provide a possible molecular substrate for heterosynaptic plasticity.

In a previous paper, we introduced a simple model of CaMKII translocation waves based on a system of reaction–diffusion equations identical in form to the diffusive SI model, which was originally used to model the spread of bubonic plague (Noble 1974). Following Rose et al. (2009), we assumed that CaMKII exists in either a primed (P) or activated (A) state and only the latter can translocate into spines. We derived a simple formula for the speed of translocation waves given by $c = 2\sqrt{D(k-h)}$, where D is the cytosolic diffusivity of CaMKII, k is the effective activation rate for the irreversible reaction $A + P \to 2A$, and h is the global translocation rate. One prediction of our model was that wave propagation failure could occur if the density of spines ρ were too high, assuming that h is proportional to ρ. A major simplification of our previous model was to treat the distribution of spines as spatially uniform. However, there are at least two sources of heterogeneity in the spine distribution that occur on two different spatial scales. First, spines are discrete entities that are joined to a dendritic branch via a thin spine neck of submicron radius, resulting in spatial variations in spine density at the micron level. This discrete structure can be incorporated into a model of a spiny dendrite by taking ρ to be a sum of Dirac delta functions. Homogenization theory can then be used to analyze how the discrete nature of spines effects processes on larger spatial scales, such as variations in voltage/conductances (Meunier and d'Incamps 2008) and the distribution of protein receptors (Bressloff 2009) along a spiny dendrite. The second source of heterogeneity occurs on a much longer length scale that is comparable to the length of a dendrite, which can vary from 100 μm to a few millimeters. The latter heterogeneity reflects the experimental observation that there is a slow proximal to distal variation in the density of spines (Konur et al. 2003; Ballesteros-Yanez et al. 2006). In this paper, we analyze how both sources of heterogeneity modulate the speed of CaMKII translocation waves along a spiny dendrite.

The structure of the paper is as follows. In Sect. 2, we briefly describe our previous model of translocation waves (Earnshaw and Bressloff 2010) and summarize some of the predictions of the model. In Sect. 3, we extend the formulation of pulsating waves by Shigesada et al. (1986) in order to take into account the discrete nature of spines. We then use homogenization theory to derive an approximate formula for the wavespeed as a function of the spine spacing (Sect. 4). Finally, in Sect. 5, we use the Hamilton–Jacobi formulation to analyze the effects of a slowly varying spine density.

2 Model of CaMKII translocation waves

Our previous mathematical model of CaMKII translocation waves within a dendrite (Earnshaw and Bressloff 2010) is based upon an experimentally motivated mechanism proposed by Rose et al. (2009), which is illustrated in Fig. 2. The model is given by a system of reaction–diffusion equations for the concentrations of activated and primed CaMKII along a uniform one-dimensional non-branching dendritic cable. These equations incorporate three major components of the dynamics: *diffusion* of CaMKII along the dendrite, *activation* of primed CaMKII, and *translocation* of activated CaMKII from the dendrite to spines (Earnshaw and Bressloff 2010):

$$\frac{\partial P}{\partial t} = D\frac{\partial^2 P}{\partial x^2} - k_0 A P \tag{2.1}$$

$$\frac{\partial A}{\partial t} = D\frac{\partial^2 A}{\partial x^2} + k_0 A P - hA. \tag{2.2}$$

Here D is the diffusivity of CaMKII within the cytosol, $P(x,t)$ and $A(x,t)$ denote the concentration of primed and activated CaMKII at time $t > 0$ and location x along the dendrite. The reaction term $k_0 AP$ represents the conversion of CaMKII from its primed to active state based on the irreversible first-order reaction scheme

$$A + P \to 2A$$

with mass action kinetics, where k_0 is the rate at which primed CaMKII is activated per unit concentration of activated CaMKII. The decay term hA represents the loss of activated CaMKII from the dendrite due to translocation into a uniform distribution of spines at a rate h. Translocation is taken to be irreversible over the time-scale of experimental or numerical observations, which is reasonable given that activated CaMKII accumulation at synapses can persist for several minutes (Shen and Meyer 1999). We assume that all of the CaMKII within the stimulated region is instantaneously activated at $t = 0$, but none has yet translocated into spines nor diffused into the non-stimulated region. We also neglect any delays associated with priming CaMKII along the remainder of the dendrite, thus avoiding the need to model explicitly the Ca^{2+} spike, see Fig. 2. This is a reasonable approximation, since the Ca^{2+} spike travels much faster than the CaMKII translocation wave (Rose et al. 2009). Thus by the time a significant amount of activated CaMKII has diffused into non-stimulated regions of the dendrite, any CaMKII encountered there will already be primed. Note, however, that once could develop a more detailed model that takes into account the initial transient associated with the priming phase by coupling the reaction–diffusion equations with additional model equations describing fast propagating Ca^{2+} spikes (see Baer and Rinzel 1991; Coombes and Bressloff 2000, 2003).

Note that Eqs. (2.1) and (2.2) are identical in form to the diffusive SI model introduced by Noble (1974) to explain the spread of bubonic plague through Europe in the fourteenth century. In the latter model, $P(x,t)$ and $A(x,t)$ would represent the densities of susceptible and infective people at spatial location x at time t, respectively, k_0 would be the transmission rate and h the death rate. In the absence of

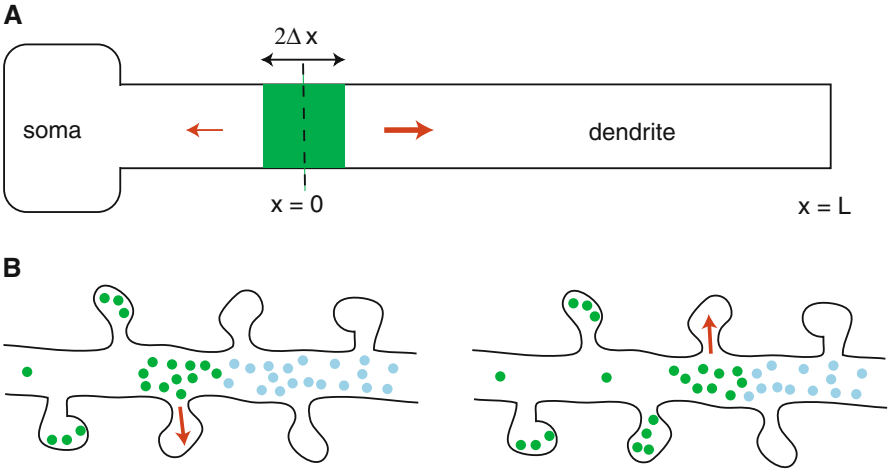

Fig. 2 Proposed mechanism of CaMKII translocation waves. **a** Glutamate/glycine puff activates CaMKII locally and initiates a fast Ca^{2+} spike that propagates distally (indicated by *larger red arrow*) and primes CaMKII in the remainder of the dendrite. In certain cases one also finds a second wave propagating proximally from the stimulated site to the soma (indicated by *smaller red arrow*). **b** Activated CaMKII (*green dots*) both translocates into spines (*red arrows*) and diffuses into distal regions of the dendrite where it activates primed CaMKII (*blue dots*). The net effect is a wave of translocated CaMKII propagating along the dendrite (color figure online)

translocation into spines ($h = 0$), the total amount of CaMKII is conserved so that $A(x,t) + P(x,t) = P_0$ for all x and $t \geq 0$. Equations (2.1) and (2.2) then reduce to the scalar Fisher–Kolmogorov et al. (F-KPP) equation

$$\frac{\partial A}{\partial t} = D\frac{\partial^2 A}{\partial x^2} + k_0 A(P_0 - A), \tag{2.3}$$

which was originally introduced to model the invasion of a gene into a population. The F-KPP equation and its generalizations have been widely used to describe the spatial spread of invading species including plants, insects, genes and diseases (see for example, Murray 1989; Holmes et al. 1994; Shigesada and Kawasaki 1997; Volpert and Petrovskii 2009 and references therein). One characteristic feature of such equations is that they support traveling fronts propagating into an unstable steady state, in which the wavespeed and long-time asymptotics are determined by the dynamics in the leading edge of the wave—so-called pulled fronts (van Saarloos 2003). In particular, a sufficiently localized initial perturbation (such as the stimulus used to generate CaMKII waves) will asymptotically approach the traveling front solution that has the minimum possible wavespeed.

A traveling wave solution of Eqs. (2.1) and (2.2) takes the form $P(x,t) = P(\xi)$ and $A(x,t) = A(\xi)$, $\xi = x - ct$, where c, $c > 0$, is the wavespeed, such that

$$P(\xi) \to P_0, \ A(\xi) \to 0 \quad \text{as } \xi \to \infty$$

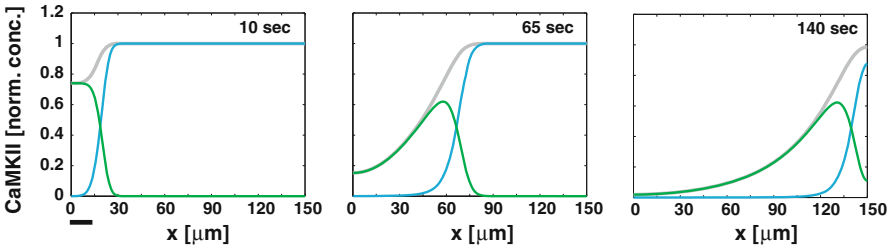

Fig. 3 Three successive snapshots of a numerically simulated translocation wave propagating along a homogeneous dendrite. Solutions of Eqs. (2.1) and (2.2) are plotted for parameter values consistent with experimental data on CaMKIIα (Shen et al. 1998; Shen and Meyer 1999; Rose et al. 2009). The translocation rate $h = 0.05$/s, diffusivity $D = 1\ \mu\text{m}^2$/s and the activation rate $k_0 P_0 = 0.21$/s. At time $t = 0$ all of the CaMKII within the stimulated region (indicated by *thick bar*) is in the activated state, whereas all of the CaMKII within the nonstimulated region is in the primed state. Concentrations are normalized with respect to the initial concentration of primed CaMKII. Composite wave consists of a pulse of activated CaMKII (*green curve*) moving at the same speed as a front of primed CaMKII (*blue curve*). Also shown is the total CaMKII concentration along the dendrite (*thick gray curve*), which decreases with time due to translocation into spines. The front forms an interface between a quiescent region containing a uniform concentration of primed CaMKII and a region dominated by translocation of activated CaMKII into spines. The dynamics in the interfacial region is dominated by diffusion-activation of primed CaMKII (color figure online)

and

$$P(\xi) \to P_1 < P_0,\ A(\xi) \to 0 \quad \text{as}\, \xi \to -\infty.$$

Here P_1 is the residual concentration of primed CaMKII following translocation of activated CaMKII into spines. The minimum wavespeed can be calculated by substituting the traveling wave solution into Eqs. (2.1) and (2.2) and linearizing near the leading edge of the wave where $P \to P_0$ and $A \to 0$. Requiring that the solution remains positive within the leading edge then shows that a traveling wave solution with speed c only exists if (Earnshaw and Bressloff 2010)

$$c \geq c_{\min} = 2\sqrt{D(k-h)}, \tag{2.4}$$

which implies that $k > h$. An example of a numerically determined traveling wave solution with minimal speed $c_{\min}$ is shown in Fig. 3 for parameter values consistent with experimental studies of CaMKIIα. In particular, $D \sim 1\ \mu\text{m}^2$/s, $h \sim 0.05\ \text{s}^{-1}$ and $c \sim 1\ \mu$m/s (Shen et al. 1998; Shen and Meyer 1999; Rose et al. 2009) for CaMKIIα; CaMKIIβ has a diffusivity and translocation rate an order of magnitude smaller but exhibits comparable wavespeeds. Our formula for the wavespeed then gives an estimate for the unknown activation rate, $k \sim 0.2\ \text{s}^{-1}$. It can be seen in Fig. 3 that the wave profile of primed CaMKII is in the form of a front, whereas the comoving wave profile of activated CaMKII is a localized pulse.

The above analysis predicts wave propagation failure when the translocation rate h is greater than the effective activation rate k. Experimentally, h is determined by globally activating CaMKII along a dendrite and determining the rate at which the level of CaMKII decays (Shen et al. 1998; Shen and Meyer 1999). The detailed

microscopic mechanism whereby CaMKII is translocated into spines is currently not known, so it is difficult to relate h to individual spine properties. In our previous paper, we assumed that the translocation rate depends on the spine density according to $h = \rho v_0$, where v_0 is an effective "velocity" associated with translocation into an individual spine. Since the activation rate can be expressed as $k = k_0 P_0$, where P_0 is the initial concentration of primed CaMKII in the nonstimulated region of the dendrite, our model predicts that CaMKII translocation waves will fail to propagate when

$$\rho v_0 > k_0 P_0. \tag{2.5}$$

For example, this inequality predicts that dendrites with a high density of spines are less likely to exhibit translocation waves than those with a low spine density. It also predicts that dendrites with a larger initial concentration of primed CaMKII in the shaft are more likely to exhibit translocation waves than those with a smaller initial concentration. Since the initial concentration P_0 of primed CaMKII depends on the effectiveness of the Ca^{2+} spike in both propagating along the dendrite and priming the inactive state, our model agrees with the experimental finding that translocation waves fail to propagate when L-type Ca^{2+} channels are blocked (Rose et al. 2009). One also finds that Ca^{2+} spikes are less likely to propagate towards the soma, which could explain why translocation waves are more often observed propagating towards the distal end of a dendrite.

3 Pulsating waves in the presence of discretely distributed spines

One of the major simplifications of the above model is that the discrete nature of dendritic spines is ignored by treating the spine density ρ and, hence, the translocation rate h, as uniform. Given the fact that the radius of the spine neck is typically at the submicron level, which is much smaller than any other length scale of the system, we can take into account the discreteness of spines by representing the spine density as a sum of Dirac delta functions (Coombes and Bressloff 2003; Bressloff and Earnshaw 2007; Meunier and d'Incamps 2008; Bressloff 2009):

$$\rho(x) = \sum_{n\in\mathbb{Z}} \delta(x - x_n), \tag{3.1}$$

where x_n is the location of the nth spine along the dendrite. It immediately follows that the translocation rate h is itself space-dependent and Eqs. (2.1) and (2.2) become heterogeneous. In this paper we are interested in the effects of spine discreteness on CaMKII translocation waves. In particular, we focus on the case of spine clusters that are uniformly spaced with $x_n = n\Delta$ where Δ is the spine cluster spacing, and there are $\overline{n}$ spines in a cluster. In order to separate the effects of discreteness from the effects of spine density, we will assume that the size of a cluster scales with Δ so that $\overline{n} = \overline{\rho}\Delta$ with $\overline{\rho}$ fixed, see Fig. 4. Thus, setting $\overline{h} = \overline{\rho} v_0$, we have the space-dependent

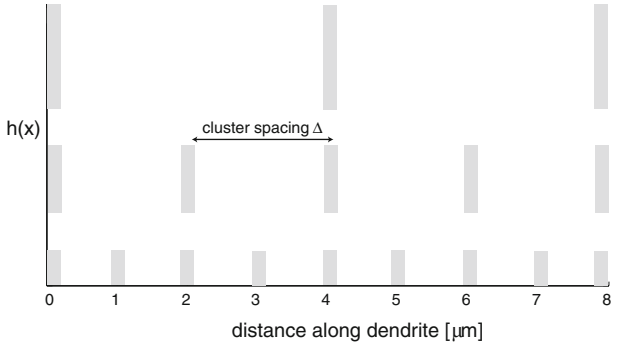

Fig. 4 Spine clustering. Plot of inhomogeneous translocation rate $h(x)$ for various cluster spacings Δ. The effective translocation rate (number of spines in a cluster) at each site is indicated by the *height of the corresponding bar*

translocation rate

$$h(x) = \overline{h}\Delta \sum_{n\in\mathbb{Z}} \delta(x - n\Delta), \tag{3.2}$$

such that $L^{-1}\int_0^L h(x)dx = \overline{h}$ for $L \gg \Delta$.

In recent years, there has been an increasing interest in studying biological invasion in heterogeneous environments using reaction–diffusion equations (Gartner and Freidlin 1979; Shigesada et al. 1986; Shigesada and Kawasaki 1997; Xin 2000; Weinberger 2002; Kinezaki et al. 2003; Cantrell and Cosner 2003; Berestycki et al. 2005; El Smaily et al. 2009). Heterogeneity is often incorporated by assuming that the diffusion coefficient and the growth rate of a population are periodically varying functions of space. One of the simplest examples of a single population model in a periodic environment was proposed by Shigesada et al. (Shigesada et al. 1986; Shigesada and Kawasaki 1997), in which two different homogeneous patches are arranged alternately in one-dimensional space so that the diffusion coefficient and the growth rate are given by periodic step functions. The authors showed numerically that an invading population starting from a localized perturbation evolves to a traveling periodic wave in the form of a pulsating front. The population density $u(x,t)$ of such a wave is defined by the condition $u(x,t) = u(x+\sigma, t+T)$ such that $\lim_{x\to\infty} u(x,t) = 0$ and $\lim_{x\to-\infty} u(x,t) = p(x)$, where $p(x)$ is a spatially periodic stationary solution of the corresponding reaction–diffusion equation. This form of solution repeats itself in a time interval T if it is observed at two successive points separated by a distance σ. The speed of the wave is then taken to be $c = \sigma/T$. Shigesada et al. (1986) also used linearized information within the leading edge of the pulsating front to derive wavespeed estimates, generalizing the analysis of pulled fronts in homogeneous media (van Saarloos 2003). An interesting recent extension of this approach has been used to study pulsating fronts in periodically modulated nonlocal neural field equations (Coombes and Laing 2011). The theory of pulsating fronts has also been developed in

a more general and rigorous setting (Gartner and Freidlin 1979; Xin 2000; Weinberger 2002; Berestycki et al. 2005; El Smaily et al. 2009).

We follow the basic formulation of Shigesada et al. (1986) by linearizing Eq. (2.2) at the leading edge of the wave where $A(x,t) \to 0$ and $P(x,t) \to P_0$:

$$\frac{\partial A}{\partial t} = D\frac{\partial^2 A}{\partial x^2} + kA - h(x)A, \tag{3.3}$$

with $h(x)$ given by the Δ-periodic function (3.2). Assume a solution of the form $A(x,t) = a(\xi)P(x)$, $\xi = x - ct$, and set

$$\frac{\partial}{\partial t} \to -c\frac{\partial}{\partial \xi}, \quad \frac{\partial}{\partial x} \to \frac{\partial}{\partial x} + \frac{\partial}{\partial \xi}.$$

Substitution into Eq. (3.3) then gives

$$\begin{aligned} -cP(x)a'(\xi) = D\left[a''(\xi)P(x) + 2a'(\xi)P'(x) + a(\xi)P''(x)\right] \\ + [k - h(x)]a(\xi)P(x). \end{aligned} \tag{3.4}$$

Dividing through by $a(\xi)P(x)$ and rearranging yields

$$D\frac{a''(\xi)}{a(\xi)} + \left[2D\frac{P'(x)}{P(x)} + c\right]\frac{a'(\xi)}{a(\xi)} = -D\frac{P''(x)}{P(x)} - k + h(x). \tag{3.5}$$

Applying the operator $\partial_x \partial_\xi$ to both sides of Eq. (3.5) implies that either $P'(x)/P(x)$ is a constant or $a'(\xi)/a(\xi)$ is a constant. Only the latter condition is consistent with $P(x)$ being a periodic function. Thus, $a(\xi) = A_0 \mathrm{e}^{-\lambda\xi}$ with λ determined by solutions to the damped Hill equation

$$P''(x) - 2\lambda P'(x) + \left[\lambda^2 + \frac{k - h(x) - c\lambda}{D}\right]P(x) = 0. \tag{3.6}$$

Note that if we set $P(x) = \mathrm{e}^{\lambda x}U(x)$ then $U(x)$ satisfies the undamped Hill equation

$$DU''(x) + [k - h(x) - c\lambda]\,U(x) = 0. \tag{3.7}$$

In order to determine the minimal wavespeed $c_{\min}$, it is necessary to find a bounded periodic solution $P(x)$ of Eq. (3.6), which yields a corresponding dispersion relation $c = c(\lambda)$, whose minimum with respect to λ can then be determined (assuming it exists). Unfortunately, for general periodic functions $h(x)$ it is not possible to solve Eq. (3.6) explicitly, and some form of approximation scheme is required. We will proceed by exploiting the fact that the spine cluster spacing Δ is at least an order of magnitude smaller than the width of the traveling wave of the homogeneous system. This will allow us to extend a recent homogenization scheme for analyzing the discrete effects of spines, which has previously been applied to studying variations in electrical voltage/conductance (Meunier and d'Incamps 2008) and the distribution of

protein receptors (Bressloff 2009) along spiny dendrites. Interestingly, El Smaily et al. (2009) independently applied the same homogenization procedure to analyze wave-speed in the population model of Shigesada et al. (1986). A more general discussion of homogenization techniques applied to traveling fronts can be found in the review by Xin (2000).

4 Homogenization of pulsating waves for a fast periodic modulation of spine density

As a first step, we introduce a macroscopic length scale σ and set $\Delta = \varepsilon\sigma$ with $\varepsilon \ll 1$. We identify σ with the effective width of the primed CamKII front, which turns out to be around 20–30 μm in the given parameter regimes. Equation (3.7) can then be rewritten in the form

$$\frac{d^2U}{dx^2} + \left[\overline{\Gamma} - \Delta\Gamma\left(\frac{x}{\varepsilon}\right)\right]U(x) = 0, \tag{4.1}$$

where

$$\overline{\Gamma} = \left[k - c\lambda - \overline{h}\right]/D \tag{4.2}$$

and

$$\Delta\Gamma(y) = \frac{\overline{h}}{D}\left(\sigma\sum_{n\in\mathbb{Z}}\delta(y - n\sigma) - 1\right) \tag{4.3}$$

such that $\Delta\Gamma(y)$ is a σ-periodic function of y. The basic idea of multi-scale homogenization is to expand the solution of Eq. (4.1) as a power series in ε, with each term in the expansion depending explicitly on the "slow" (macroscopic) variable x and the "fast" (microscopic) variable $y = x/\varepsilon$ (Meunier and d'Incamps 2008; Bressloff 2009; El Smaily et al. 2009):

$$U(x, y) = U_0(x) + \varepsilon U_1(x, y) + \varepsilon^2 U_2(x, y) + \cdots, \tag{4.4}$$

where $U_j(x, y)$, $j = 1, \ldots$ are σ-periodic in y. The perturbation series expansion is then substituted into Eq. (4.1) with x, y treated as independent variables so that derivatives with respect to x are modified according to $\partial_x \to \partial_x + \varepsilon^{-1}\partial_y$. This generates a hierarchy of equations corresponding to successive powers of ε:

$$\frac{\partial^2 U_1}{\partial y^2} = 0 \tag{4.5}$$

$$\frac{d^2U_0}{dx^2} + 2\frac{\partial^2 U_1}{\partial x\,\partial y} + \frac{\partial^2 U_2}{\partial y^2} + \left[\overline{\Gamma} - \Delta\Gamma(y)\right]U_0 = 0 \tag{4.6}$$

at powers ε^{-1}, 1 and

$$\frac{\partial^2 U_n}{\partial x^2}+2\frac{\partial^2 U_{n+1}}{\partial x\partial y}+\frac{\partial^2 U_{n+2}}{\partial y^2}+\left[\overline{\Gamma}-\Delta\Gamma(y)\right]U_n=0 \tag{4.7}$$

at $\mathcal{O}(\varepsilon^n)$, $n\geq 1$.

Equation (4.5) and boundedness of U_1 imply that U_1 is independent of y, and can thus be absorbed into $U_0(x)$. Thus the leading order corrections arising from small-scale fluctuations in the spine density occur at $\mathcal{O}(\varepsilon^2)$. Define the spatial average of a periodic function $F(y)$, denoted by $\langle F\rangle$, according to

$$\langle F\rangle=\frac{1}{\sigma}\int_0^\sigma F(y)dy. \tag{4.8}$$

Taking the spatial average of Eq. (4.6) with $U_0=\langle U_0\rangle$ then gives

$$\frac{d^2U_0}{dx^2}+\overline{\Gamma}U_0=0. \tag{4.9}$$

We have exploited the fact that U_2 is periodic in y so $\langle\partial^2U_2/\partial y^2\rangle=0$. In order to calculate U_2, we first subtract the averaged Eq. (4.9) from (4.6) to obtain

$$\frac{\partial^2U_2}{\partial y^2}=\Delta\Gamma(y)U_0(x). \tag{4.10}$$

It follows that $U_2(x,y)=U_0(x)\chi(y)$ with $\chi''(y)=\Delta\Gamma(y)$ and χ a σ-periodic function of y. Integrating once with respect to y gives $\chi'(y)=\chi'(0)+\int_0^y\Delta\Gamma(z)dz$. We can eliminate the unknown $\chi'(0)$ by spatially averaging with respect to y and using $\langle\chi'\rangle=0$. This gives $\chi'(y)=\oint_0^y\Delta\Gamma(z)dz$ with

$$\oint_0^y f(z)dz\equiv\int_0^y f(z)dz-\left\langle\int_0^y f(z)dz\right\rangle \tag{4.11}$$

for any integrable function f. Another integration with respect to y shows that

$$\chi(y)=\chi(0)+\int_0^y\oint_0^{y'}\Delta\Gamma(z)dzdy'.$$

Spatially averaging this equation with respect to y in order to express $\chi(0)$ in terms of $\langle\chi\rangle$ and multiplying through by $U_0(x)$, finally gives

$$\begin{aligned}\Delta U_2(x,y) &\equiv U_2(x,y) - \langle U_2\rangle(x)\\ &= U_0(x)\oint_0^y\oint_0^{y'}\Delta\Gamma(z)dzdy'.\end{aligned}\tag{4.12}$$

It remains to determine the equation satisfied by $\langle U_2\rangle$. Spatially averaging Eq. (4.7) for $n=2$ gives

$$\frac{d^2\langle U_2\rangle}{dx^2} + \overline{\Gamma}\langle U_2\rangle = \langle\Delta\Gamma(y)U_2(x,y)\rangle.\tag{4.13}$$

Substituting Eq. (4.12) into (4.13) and reordering the resulting multiple integral yields the result

$$\frac{d^2\langle U_2\rangle}{dx^2} + \overline{\Gamma}\langle U_2\rangle = -\left\langle\left(\oint_0^y\Delta\Gamma(z)dz\right)^2\right\rangle U_0(x).\tag{4.14}$$

Finally, writing $\langle U\rangle = U_0 + \varepsilon\langle U_2\rangle + \cdots$ we obtain the homogenized version of the Hill equation (3.7):

$$\frac{d^2\langle U\rangle}{dx^2} + \Gamma_\varepsilon\langle U\rangle = 0,\tag{4.15}$$

where

$$\Gamma_\varepsilon = \overline{\Gamma} - \varepsilon^2\Gamma_2 + \mathcal{O}(\varepsilon^3),\quad \Gamma_2 = \left\langle\left(\oint_0^y\Delta\Gamma(z)dz\right)^2\right\rangle.\tag{4.16}$$

Recall that we require the solution $P(x) = \mathrm{e}^{\lambda x}U(x)$ to be a bounded periodic function of x. It follows that $\langle P\rangle = \mathrm{e}^{\lambda x}\langle U(x)\rangle$ should be a finite constant. Writing the solution of equation (4.15) as $\langle U(x)\rangle \sim \mathrm{e}^{-\sqrt{\Gamma_\varepsilon}x}$, we obtain the characteristic equation

$$\lambda = \sqrt{\frac{c\lambda - k + \overline{h}}{D} - \varepsilon^2\Gamma_2},\tag{4.17}$$

where we have substituted for $\overline{\Gamma}$ using Eq. (4.2). Squaring both sides and rearranging thus leads to the following dispersion relation for the wavespeed c:

$$c = c(\lambda) \equiv D\lambda + \frac{k - \overline{h} + \varepsilon^2 D\Gamma_2}{\lambda}.\tag{4.18}$$

Minimizing with respect λ then shows that

$$c_{\min} = 2\sqrt{D(k-\overline{h}) + \varepsilon^2 D^2 \Gamma_2}, \tag{4.19}$$

For sufficiently small ε, we can Taylor expand equation (4.19) to obtain the further approximation

$$c_{\min} \approx \overline{c} + \frac{2D^2\Gamma_2}{\overline{c}}\varepsilon^2, \tag{4.20}$$

with $\overline{c} = 2\sqrt{D(k-\overline{h})}$ the wavespeed of the corresponding homogeneous distribution of spines. Hence, we have shown that a periodic variation in the spine density due to clustering leads to an $\mathcal{O}(\varepsilon^2)$ increase in the wavespeed. An analogous result was obtained by El Smaily et al. (2009) for the Shigesada et al. model (Shigesada et al. 1986). Equation (4.12) implies that there are also small-scale fluctuations of the wave profile in the leading edge of the wave given by:

$$\frac{\Delta P(y)}{\langle P\rangle} = \varepsilon^2 \oint_0^y \oint_0^{y'} \Delta\Gamma(z)dzdy' + \mathcal{O}(\varepsilon^3). \tag{4.21}$$

It is straightforward to calculate the integrals in Eqs. (4.19) and (4.21) for a periodic spine density with $\Delta\Gamma(y)$ given by Eq. (4.3) (Meunier and d'Incamps 2008):

$$\Gamma_2 = \left\langle \left(\oint_0^y \Delta\Gamma(z)dz \right)^2 \right\rangle = \frac{1}{12}\left(\frac{\overline{h}\sigma}{D}\right)^2, \tag{4.22}$$

$$\oint_0^y \oint_0^{y'} \Delta\Gamma(z)dzdy' = \frac{\overline{h}\sigma^2}{D}\left[\frac{y}{2\sigma} - \frac{y^2}{2\sigma^2} - \frac{1}{12}\right]. \tag{4.23}$$

Since $\varepsilon = \Delta/\sigma$, it follows that fluctuations in the wave profile vary between $-\overline{h}\Delta^2/(12D)$ at spine clusters and $\overline{h}\Delta^2/(24D)$ between spine clusters, and

$$c_{\min} = 2\sqrt{D(k-\overline{h}) + \Delta^2\overline{h}^2/12}. \tag{4.24}$$

It immediately follows that for fixed $\overline{h}$, k, D (and hence $\overline{c}$), spine clustering increases the speed of a translocation wave. This is illustrated in Fig. 5, where we plot the minimal wavespeed $c_{\min}$ given by Eq. (4.24) as a function of the activation rate k for various values of the cluster spacing Δ. An additional important consequence of clustering is that it reduces the threshold for the existence of a translocation wave. That is, there exists a critical value of the activation rate, $k = \kappa(\Delta)$, below which translocation waves do not exist and $\kappa(\Delta)$ is a decreasing function of Δ. In the homogenization limit $\Delta \to 0$, we recover the result $\kappa = \overline{h}$.

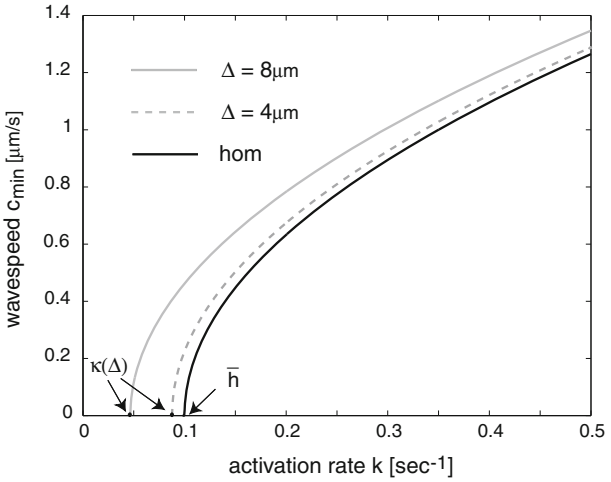

Fig. 5 Plot of minimal wavespeed $c_{\min}$ as a function of activation rate $k = k_0 P_0$ for various values of the spine cluster spacing Δ. Also shown is the corresponding wavespeed for a homogeneous spine distribution (*black curve*). Other parameters are $\overline{h} = 0.1\ \mathrm{s}^{-1}$ and $D = 1\ \mu\mathrm{m}^2/\mathrm{s}$. Note that wave propagation failure occurs as $k \to \kappa(\Delta)$ from above where $\kappa(\Delta)$ is the propagation threshold

The existence of a pulsating wave due to spine clustering and the associated increase (decrease) in the minimal speed (threshold) of the wave can also be confirmed numerically. For the sake of illustration, we take a dendrite of length $L = 300\ \mu\mathrm{m}$ with reflecting boundary conditions at both ends $x = 0, L$. The initial conditions are given by

$$P(x,0) = P_0,\ A(x,0) = 0 \quad \text{for all } x \notin [0, \delta L]$$
$$P(x,0) = 0,\ A(x,0) = P_0 \quad \text{for all } x \in [0, \delta L],$$

with $\delta L = 15\mu\mathrm{m}$. We discretize space by setting $x = m\delta x$, where δx is the step length and $m = 0, 1, \ldots, M$ with $M = L/\delta x$. In discrete spatial units the spine cluster spacing is taken to be $\Delta = P\delta x$. The spine cluster distribution is then represented numerically by the discrete sum

$$\rho(m\delta x) = \frac{1}{\delta x} \sum_{j=0}^{M/P} \delta_{m,jP}, \tag{4.25}$$

where $\delta_{m,j}$ is the Kroenecker delta and δx is chosen so that M, P and M/P are integers. The spatially discretized version of Eqs. (2.1) and (2.2) are then solved in Matlab (MathWorks) using standard differential equation solvers. Examples of numerical solutions are shown in Figs. 6, 7, 8 for $\overline{h} = 0.1/\mathrm{s}$ and $k = 0.19/\mathrm{s}$. In each figure, we plot concentration profiles at four successive snapshots in time, following stimulation of a local region of dendrite at an initial time $t = 0$. We focus on the spread of CaMKII distally from the site of stimulation. Comparison between waves for a

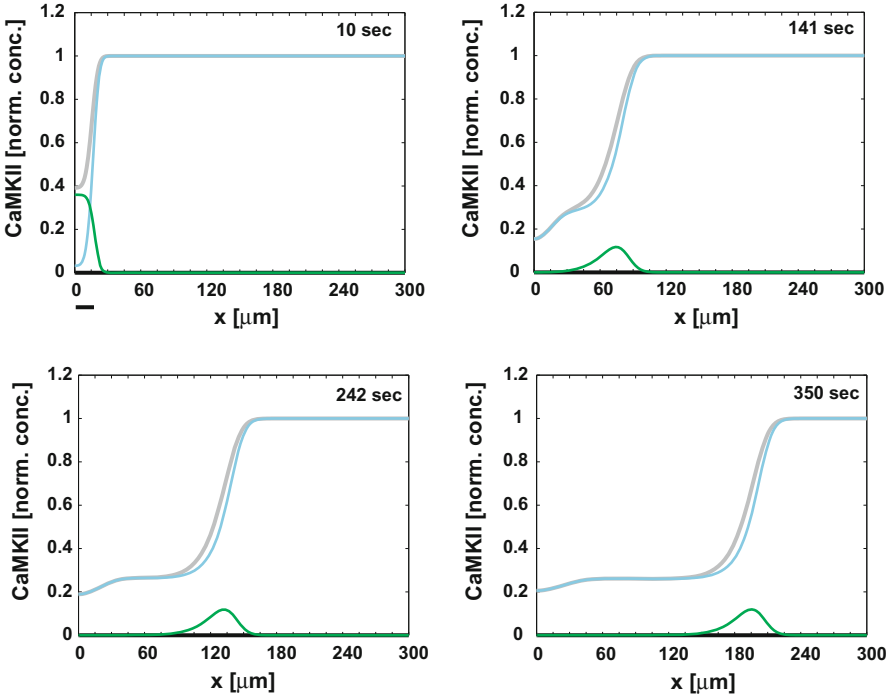

Fig. 6 Numerical traveling wave solution of Eqs. (2.1) and (2.2) for a homogeneous (uniform) distribution of spines. The translocation rate $\overline{h} = 0.1$/s, diffusivity $D = 1\ \mu\text{m}^2$/s and the activation rate $k = 0.19$/s. At time $t = 0$ all of the CaMKII within the stimulated region (indicated by *thick bar*) is in the activated state, whereas all of the CaMKII within the nonstimulated region is in the primed state. Concentrations are normalized with respect to the initial concentration of primed CaMKII. The resulting wave profiles for activated (*green curve*) and primed (*blue curve*) CaMKII along the dendrite are shown at four successive snapshots in time. Also shown is the total CaMKII concentration along the dendrite (*thick gray curve*), which decreases with time due to translocation into spines. The numerically estimated wavespeed $c_{\min} \approx 0.58\ \mu$m/s, which is close to the predicted wavespeed $\overline{c} = 0.6\ \mu$m/s (color figure online)

spatially uniform distribution of spines and a spatially discrete distribution of spine clusters shows that the wave is periodically modulated and faster in the latter case. This is a consequence of the fact that translocation is less effective in the presence of spine clusters. Although doubling the degree of clustering only leads to a change in wavespeed of order 0.05 μm/s (consistent with our analytical calculations), it leads to a significant difference in propagation times along a 300 μm dendrite. In Figs. 9, 10, 11, we illustrate the effect of spine clustering on lowering the threshold for wave propagation by taking $\overline{h} = 0.1$/s and $k = 0.1$/s. In this case, since $k = \overline{h}$, no wave propagates for a homogeneous spine distribution as can be seen in Fig. 9. That is, activated CaMKII only invades a limited region of the dendrite before the concentration decays to zero. Thus, translocation only occurs within this restricted region and in the long time limit the system returns to a uniform concentration of primed CaMKII (but at a slightly reduced level). On the other hand, in the presence of a sufficiently high degree of spine clustering (sufficiently large Δ), wave propagation is observed as shown in Figs. 10 and 11.

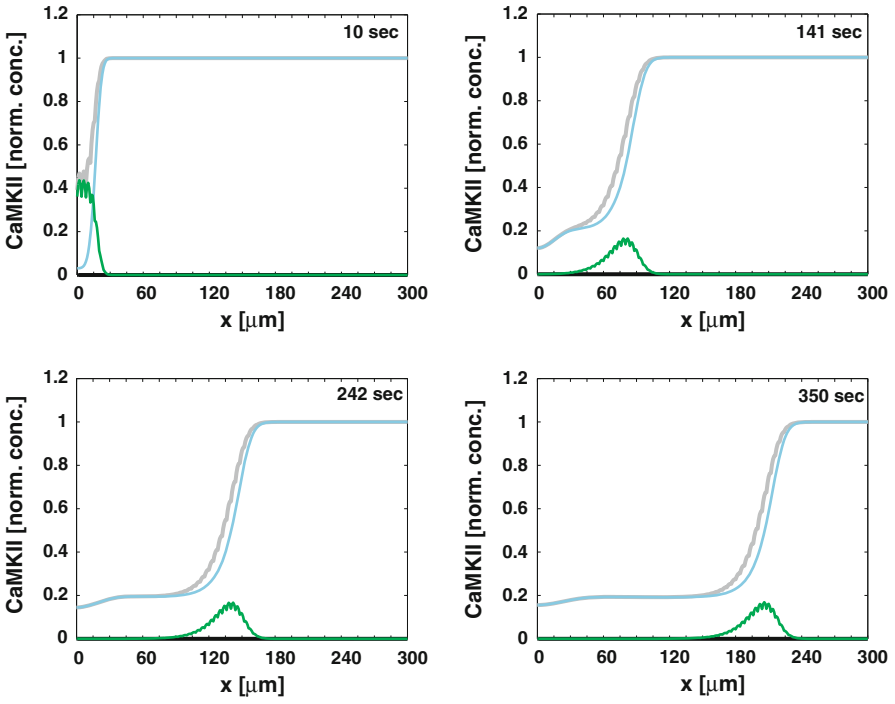

Fig. 7 Same as Fig. 6 except for an inhomogeneous distribution of spine clusters with periodic spacing $\Delta = 4$ μm. Wave is slightly faster with mean wavespeed $c_{\min} \approx 0.6$ μm/s

Finally, note that it is possible to extend the above homogenization scheme to the case of randomly rather than periodically distributed spines, provided that the resulting heterogeneous medium is *ergodic* (Torquato 2002). That is, the result of averaging over all realizations of the ensemble of spine distributions is equivalent to averaging over the length L of the dendrite in the infinite-L limit. If such an ergodic hypothesis holds and L is sufficiently large so that boundary terms can be neglected, then the above analysis carries over with $\langle\cdot\rangle$ now denoting ensemble averaging. Examples of how to evaluate integrals such as those appearing in Eqs. (4.19) and (4.21) for randomly distributed spines are presented in Meunier and d'Incamps (2008).

5 Wavespeed for a slowly modulated spine density

So far we have considered the effects of heterogeneity at a microscopic length scale comparable to the spacing of individual spines. In particular, we took the homogenized translocation rate $\bar{h}$ to be constant over the length of a dendrite. However, it is found experimentally that there is a slow proximal to distal variation in the density of spines (Konur et al. 2003; Ballesteros-Yanez et al. 2006). An illustration of a typical spine density found in pyramidal neurons of mouse cortex (Ballesteros-Yanez et al. 2006) is shown in Fig. 12. Such a variation in spine density can be incorporated into

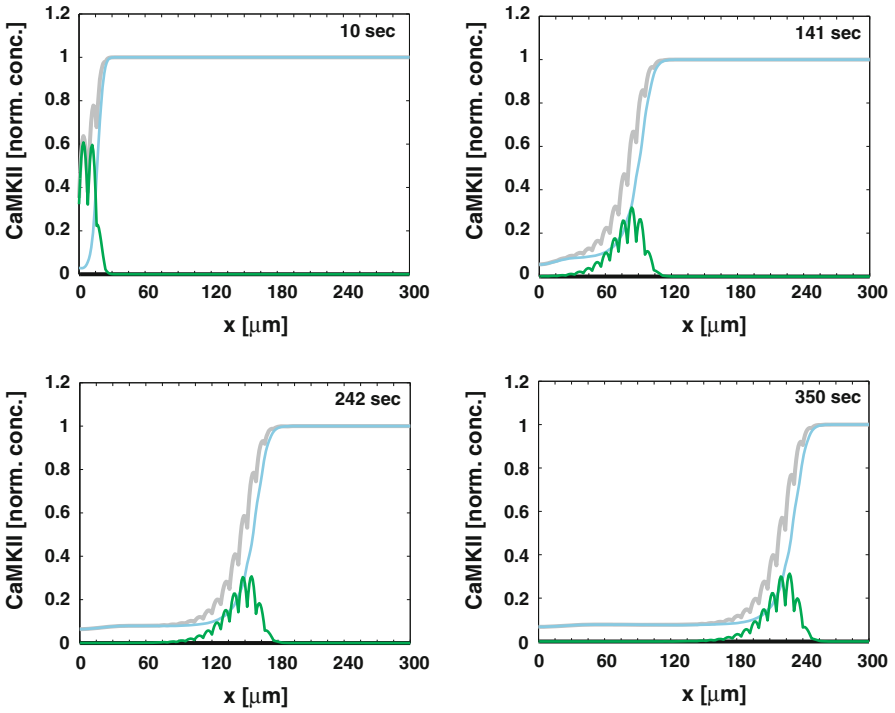

Fig. 8 Same as Fig. 7 except that $\Delta = 8$ μm. Mean wavespeed $c_{\min} \approx 0.66$ μm/s

Eqs. (2.1) and (2.2) by setting $h = \overline{h} + \Delta h(\varepsilon x)$, where $\overline{h}$ denotes the translocation rate at the initiation point x_0 of the wave and $\Delta h(\varepsilon x)$ represents the slow modulation of the (homogenized) translocation rate over the length of a dendrite with $\varepsilon \ll 1$. A different approach has been developed to study biological invasion in slowly modulated environments based on a Hamilton–Jacobi formulation. This method was originally introduced by Freidlen (Gartner and Freidlin 1979; Freidlin 1985, 1986) using large deviation theory, and subsequently formulated in terms of PDEs by Evans and Sougandis (Evans and Sougandis 1989). More recently it has been used to study waves in heterogeneous media (see for example, Xin 2000; Mendez et al. 2003). In this section we apply the Hamilton–Jacobi method to our model of CaMKII translocation waves with slow periodic modulation.

The first step in the analysis is to rescale space and time in Eqs. (2.1) and (2.2) according to $t \to t/\varepsilon$ and $x \to x/\varepsilon$ (Freidlin 1986; Evans and Sougandis 1989; Mendez et al. 2003):

$$\varepsilon \frac{\partial P}{\partial t} = D\epsilon^2 \frac{\partial^2 P}{\partial x^2} - k_0 A P \tag{5.1}$$

$$\varepsilon \frac{\partial A}{\partial t} = D\varepsilon^2 \frac{\partial^2 A}{\partial x^2} + k_0 A P - \left[\overline{h} + \Delta h(x)\right] A. \tag{5.2}$$

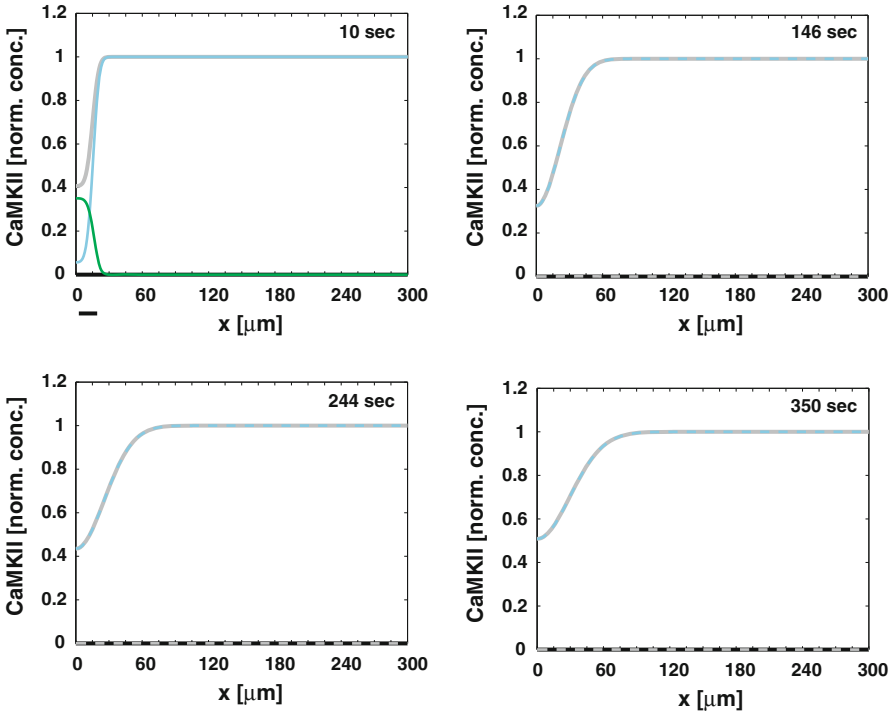

Fig. 9 Wave propagation failure for a homogeneous distribution of spines. Same as Fig. 6 except that $\overline{h} = k = 0.1\ \mathrm{s}^{-1}$. As in previous figures, at time $t = 0$ all of the CaMKII within the stimulated region (indicated by *thick bar*) is in the activated state, whereas all of the CaMKII within the nonstimulated region is in the primed state. However, activated CaMKII now only diffuses into a restricted region of size $\sim 30\ \mu\mathrm{m}$ around the induction site. Within this region some primed CaMKII is activated and translates into spines, as indicated by the reduction of total CaMKII within this region (*thick gray curve*). However, the concentration of activated CaMKII decays to zero, and in the long time limit, diffusion leads to a uniform concentration of primed CaMKII

Under the spatial rescaling the front region where P and A rapidly increase as x decreases from infinity becomes a step as $\varepsilon \to 0$, see Fig. 3. This motivates the introduction of solutions of the form

$$P(x,t) \sim P_0\left[1 - \mathrm{e}^{-G(x,t)/\varepsilon}\right], \quad A(x,t) \sim A_0(x)\mathrm{e}^{-G(x,t)/\varepsilon} \tag{5.3}$$

with $G(x,t) > 0$ for all $x > x(t)$ and $G(x(t),t) = 0$. The point $x(t)$ determines the location of the front and $c = \dot{x}$. Substituting (5.3) into Eqs. (5.1) and (5.2) gives

$$-\frac{\partial G}{\partial t} = D\left[\frac{\partial G}{\partial x}\right]^2 - D\varepsilon\frac{\partial^2 G}{\partial x^2} - k_0 A_0(x)\left[1 - \mathrm{e}^{-G(x,t)/\varepsilon}\right] \tag{5.4}$$

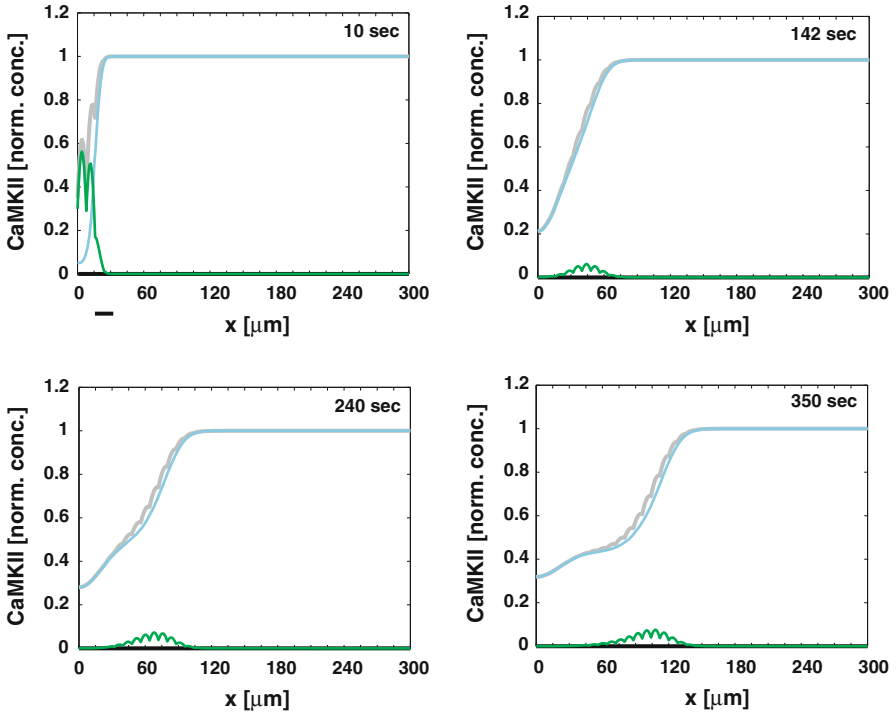

Fig. 10 Same as Fig. 9 except for an inhomogeneous distribution of spine clusters with $\Delta = 4$ μm. Although $\overline{h} = k$, a slow translocation wave with mean wavespeed $c_{\min} \approx 0.2$ μm/s now propagates. This reflects the lowering of the propagation threshold due to clustering

$$-A_0(x)\frac{\partial G}{\partial t} = A_0(x)\left[D\left[\frac{\partial G}{\partial x}\right]^2 - D\varepsilon\frac{\partial^2 G}{\partial x^2} + k_0 P_0\left[1-\mathrm{e}^{-G(x,t)/\varepsilon}\right] - \left[\overline{h}+\Delta h(x)\right]\right] + \varepsilon^2 A_0''(x)G - 2\epsilon A_0'(x)\frac{\partial G}{\partial x}. \tag{5.5}$$

To leading order in ε, these reduce to

$$-\frac{\partial G}{\partial t} = D\left[\frac{\partial G}{\partial x}\right]^2 - k_0 A_0(x) \tag{5.6}$$

$$-\frac{\partial G}{\partial t} = D\left[\frac{\partial G}{\partial x}\right]^2 + k - \left[\overline{h}+\Delta h(x)\right], \tag{5.7}$$

where $k = k_o P_0$ as before. It immediately follows that

$$A_0(x) = \left[\frac{k-\overline{h}-\Delta h(x)}{k}\right] P_0. \tag{5.8}$$

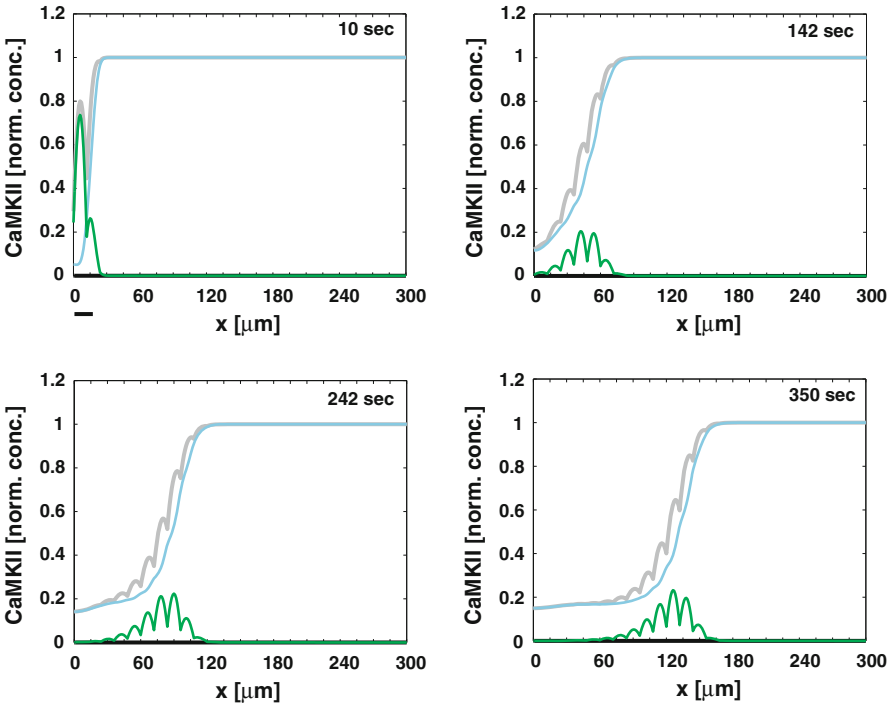

Fig. 11 Same as Fig. 10 except that $\Delta = 12$ μm. Mean wavespeed $c_{\min} \approx 0.36$ μm/s

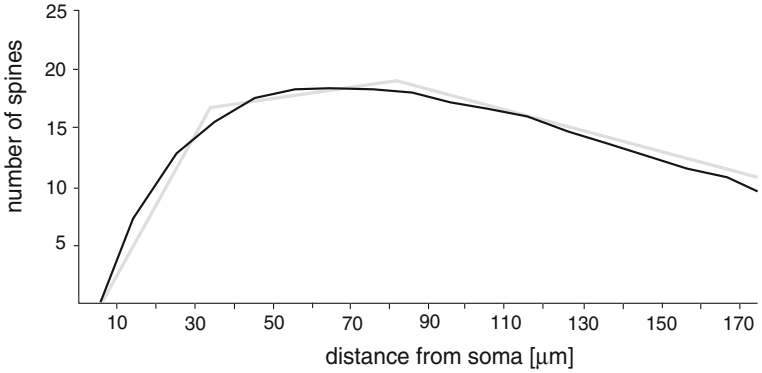

Fig. 12 Illustrative example of the spine density variation along the basal dendrite of a pyramidal cell in mouse cortex (*black curve*). Density is calculated as the number of spines per 10 μm segment of the dendrite from the soma to the tip of the dendrite. Abstracted from experimental data in Ballesteros-Yanez et al. (2006). Also shown is a simplified piecewise linear approximation of the spine density variation (*gray curve*)

The remaining Eq. (5.7) can be analyzed along identical lines to a previous study of the heterogeneous F-KPP equation (Mendez et al. 2003). Formally comparing Eq. (5.7) with the Hamilton–Jacobi equation $\partial_t G + H(\partial_x G, x) = 0$, we define the Hamiltonian

$$H = Dp^2 + k - \left[\overline{h} + \Delta h(x)\right], \tag{5.9}$$

where $p = \partial_x G$ is interpreted as the conjugate momentum of x. It now follows that Eq. (5.7) can be solved in terms of the Hamilton equations

$$\frac{dx}{ds} = 2Dp, \quad \frac{dp}{ds} = \frac{d\Delta h}{dx}. \tag{5.10}$$

Combining these equations we have the second-order ODE

$$\ddot{x} - 2D\Delta h(x)' = 0. \tag{5.11}$$

This takes the form of a Newtonian particle moving in a "potential" $V(x) = -2D\Delta h(x)$. Given the solution $x(s) = \phi(s; x, t)$ with $\phi(0; x, t) = x_0$ and $\phi(t; x, t) = x$, we can then determine $G(x, t)$ according to

$$G(x, t) = -E(x, t)t + \frac{1}{2D}\int_0^t \dot{\phi}(s; x, t)^2 ds. \tag{5.12}$$

Here

$$E(x, t) = H(\dot{\phi}(s; x, t)/2D, \phi(s; x, t)), \tag{5.13}$$

which is independent of s due to conservation of energy.

For certain choices of the modulation function $\Delta h(x)$, Eq. (5.11) can be solved explicitly (Mendez et al. 2003). In particular, suppose that the spine density curve in Fig. 3 is approximated by a piecewise linear function, in which the density increases linearly with distance from the soma to some intermediate location κ along the dendrite and then decreases linearly towards the distal end. Assuming that the right-moving wave is initiated beyond the point κ, $x_0 > \kappa$, then we can simply take $\Delta h(x) = -\beta(x - x_0)$ for $\beta > 0$. Substituting into equation (5.11) and integrating twice with respect to s using the Cauchy conditions gives

$$\phi(s; x, t) = x_0 + (x - x_0)s/t + D\beta ts - D\beta s^2. \tag{5.14}$$

The corresponding "energy" function is then

$$E(x, t) = \frac{(x - x_0)^2}{4Dt^2} + k - \overline{h} + \frac{\beta}{2}(x - x_0) + \frac{\beta^2}{4}Dt^2 \tag{5.15}$$

From equation (5.12) we then have

$$G(x, t) = \frac{(x - x_0)^2}{4Dt} - \left[k - \overline{h}\right]t - \frac{\beta}{2}(x - x_0)t - \frac{\beta^2}{12}Dt^3. \tag{5.16}$$

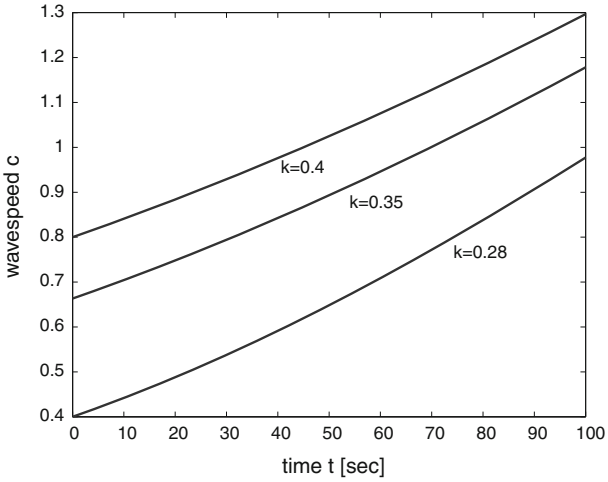

Fig. 13 Plot of time-dependent variation in wavespeed c given by Eq. (5.17) for various values of the activation rate k. Other parameters are $\overline{h} = 0.24\,\mathrm{s}^{-1}$ and $D = 1\ \mu\mathrm{m}^2/\mathrm{s}$. At $t = 0$, $c(0) = 2\sqrt{D(k-\overline{h})}$

We can now determine the wavespeed c by imposing the condition $G(x(t), t) = 0$. This leads to a quadratic equation with positive solution

$$x(t) = x_0 + D\beta t^2 + 2Dt\sqrt{\frac{k-\overline{h}}{D} + \frac{\beta^2}{3}t^2}$$
$$= x_0 + \overline{c}t\sqrt{1 + \frac{4\beta^2 D^2 t^2}{3\overline{c}^2}} + D\beta t^2$$

with $\overline{c} = 2\sqrt{D(k-\overline{h})}$. Finally, differentiating both sides with respect to t yields

$$c \equiv \dot{x}(t) = \overline{c}\sqrt{1+\Gamma_0\beta^2 t^2} + \frac{\overline{c}\Gamma_0\beta^2 t^2}{\sqrt{1+\Gamma_0\beta^2 t^2}} + 2D\beta t, \tag{5.17}$$

where $\Gamma_0 = 4D^2/(3\overline{c}^2)$. For sufficiently small times such that $D\beta t \ll 1$, we have the approximation

$$c \approx \overline{c} + 2D\beta t + \frac{2(D\beta t)^2}{\overline{c}}. \tag{5.18}$$

In Fig. 13, we show example plots of the time-dependent wavespeed for various choices of the activation rate k. It can be seen that there are significant changes in speed over a time course of 100 s, which is comparable to the time a wave would travel along a dendrite of a few hundred microns. In principle, it should be possible to test experimentally the predictions of the above analysis by initiating a translocation wave at different points along a dendrite and determining the corresponding wavespeed.

6 Discussion

In this paper we have analyzed the effects of heterogeneities in the dendritic spine distribution at several length scales on the propagation of CaMKII translocation waves along dendrites. First, we used a homogenization scheme previously applied to the study of voltage/conductance changes and protein receptor trafficking along spiny dendrites to explore the effects of spine clustering. We showed that periodically regular clustering leads to a pulsating wave that can significantly reduce the propagation time along a dendrite and the threshold for propagation failure. Second, we applied Hamilton–Jacobi theory of sharp interfaces to analyze the effects of slow variations in spine density along the length of a dendrite. In particular we obtained an estimate for the slow temporal variation of the wavespeed.

One of the potential roles of CaMKII translocation waves is in providing a signaling mechanism for long-range heterosynaptic plasticity (Frey and Morris 1997). Indeed, Rose et al. (2009) found that glutamatergic AMPA receptors coaccumulate with CaMKII in spines following the propagation of such waves. The upregulation of AMPA receptor numbers in synapses is a well-established mechanism for the expression of long-term potentiation (LTP) (Malenka and Bear 2004). On the other hand, it has also been found that inducing LTP at a single synapse activates CaMKII within the spine containing the synapse but neither induces LTP at nearby synapses nor raises CaMKII content in nearby spines (Zhang et al. 2008; Lee et al. 2009). This is consistent with our previous result that there exists an activation threshold for wave propagation, which in the case of a homogeneous spine distribution is $k = \overline{h}$. As we have shown in this paper, spine clustering reduces this threshold. One possible mechanism for wave propagation failure in the presence of weak stimulation is that the latter may fail to initiate a Ca^{2+} spike. Recall that we do not model the Ca^{2+} spike explicitly since it appears to be much faster than the CaMKII translocation wave (Rose et al. 2009). However, the effect of the Ca^{2+} spike is included in the model indirectly via the initial concentration P_0 of primed CaMKII. If a weak stimulus fails to initiate a fast Ca^{2+} spike, then $P_0 \approx 0$ for significant portions of the dendrite. In these regions the activation rate $k = k_0 P_0 \approx 0$ and so will be smaller than the translocation rate $\overline{h}$, leading to wave propagation failure in our model. One regime in which a Ca^{2+} spike could fail to propagate would be if the density of spines were too low. Thus, although low spine densities are conducive to the propagation of translocation waves, the spines must be sufficiently dense otherwise no wave will be initiated.

There is an additional source of wave propagation failure that is not taken into account by our continuum model, namely, discreteness effects associated with the number of activated and primed CaMKII holoenzymes at low CaMKII concentrations. That is, our model tracks the local concentration of CaMKII and not individual CaMKII holoenzymes. While such an approach simplifies the model, allowing one to make explicit the manner in which CaMKII translocation waves are propagated, it does neglect stochastic effects due to fluctuations in the number and location of CaMKII holoenzymes. One well known feature of pulled fronts is that they are particularly sensitive to the effects of such fluctuations in the leading edge of the front. That is, there is a fundamental quantum of activity within a local population consisting of a single activated CaMKII molecule. In other words, there is an effective lower cut-off

within the leading edge of the front. In the case of nonlinear reaction diffusion equations, such discreteness effects have been shown to have a significant effect on the asymptotic velocity of a pulled front (Brunet and Derrida 1997; Panja 2004).

Finally, from a more general biological perspective, CaMKII translocation waves are of interest because they provide an important example of how the dynamic localization of signaling proteins is used to regulate signal transduction. There have been a number of suggestions regarding the possible advantages of including a translocation step in a signaling pathway (Meyer and Shen 2000). First, it can suppress subthreshold inputs such as low Ca^{2+} concentrations by requiring stimuli to be sufficiently prolonged or strong for translocation to occur. Second, it can delay or prolong a signaling step through control of the assembly and disassembly of signaling complexes via slow diffusion and binding/unbinding of signaling molecules. Third, it can enhance specificity by allowing a high degree of regulation in the assembly of signaling complexes.

Acknowledgments This work was supported by the National Science Foundation (DMS 1120327).

References

Baer SM, Rinzel J (1991) Propagation of dendritic spikes mediated by excitable spines: a continuum theory. J Neurophysiol 65:874–890

Ballesteros-Yanez I, Benavides-Piccione R, Elston GN, Yuste R, De Felipe J (2006) Density and morphology of dendritic spines in mouse neocortex. Neuroscience 138:403–409

Barria A, Derkach V, Soderling T (1997a) Identification of the Ca^{2+}/calmodulin-dependent protein kinase II regulatory phosphorylation site in the α-amino-3-hydroxyl-5-methyl-4-isoxazole-proprionic acid glutamate receptor. J Biol Chem 272:32727–32730

Barria A, Muller D, Derkach V, Griffith LC, Soderling TR (1997b) Regulatory phosphorylation of AMPA-type glutamate receptors by CaMKII during long-term potentiation. Science 276:2042–2045

Bayer KU, De Koninck P, Leonard AS, Hell JW, Schulman H (2001) Interaction with the NMDA receptor locks CaMKII in an active conformation. Nature 411:801–805

Bayer KU et al (2006) Transition from reversible to persistent binding of CaMKII to postsynaptic sites and NR2B. J Neurosci 26:1164–1174

Berestycki H, Hamel F, Roques L (2005) Analysis of the periodically fragmented environment model: II-biological invasions and pulsating travelling fronts. J Math Biol 51:75–113

Bressloff PC, Earnshaw BA (2007) Diffusion-trapping model of receptor trafficking in dendrites. Phys Rev E 75:041915

Bressloff PC (2009) Cable theory of protein receptor trafficking in dendritic trees. Phys Rev E 79:041904

Brunet E, Derrida D (1997) Shift in the velocity of a front due to a cutoff. Phys Rev E 56:2597–2604

Cantrell RS, Cosner C (2003) Spatial ecology via reaction–diffusion equations. Wiley, Chichester

Coombes S, Bressloff PC (2000) Solitary waves in a model of dendritic cable with active spines. SIAM J Appl Math 61:432–453

Coombes S, Bressloff PC (2003) Saltatory waves in the spike-diffuse-spike model of active dendrites. Phys Rev Lett 91:4028102

Coombes S, Laing C R (2011) Pulsating fronts in periodically modulated neural field models. Phys Rev E 83:011912

Derkach V, Barria A, Soderling TR (1999) Ca^{2+}/calmodulin-kinase II enhances channel conductance of α-amino-3-hydroxyl-5-methyl-4-isoxazoleproprionate type glutamate receptors. Proc Natl Acad Sci USA 96:3269–3274

Earnshaw BA, Bressloff PC (2010) Diffusion-activation model of CaMKII translocation waves in dendrites. J Comput Neurosci 28:77–89

El Smaily M, Hamel F, Roques L (2009) Homogenization and influence of fragmentation in a biological invasion model. Discrete Contin Dyn Syst Series A 25:321–342

Evans LC, Sougandis PE (1989) A PDE approach to geometric optics for certain semilinear parabolic equations. Indiana Univ Math J 38:141–172
Fisher RA (1937) The wave of advance of advantageous genes. Ann Eugen 7:353–369
Freidlin MI (1985) Limit theorems for large deviations and reaction–diffusion equations. Ann Probab 13:639–675
Freidlin MI (1986) Geometric optics approach to reaction–diffusion equations. SIAM J Appl Math 46: 222–232
Frey U, Morris R (1997) Synaptic tagging and long-term potentiation. Nature 385:533–536
Fukunaga K, Stoppini L, Miyamoto E, Muller D (1993) Long-term potentiation is associated with an increased activity of Ca^{2+}/calmodulin-dependent protein kinase II. J Biol Chem 268:7863–7867
Fukunaga K, Muller D, Miyamoto E (1995) Increased phosphorylation of Ca^{2+}/calmodulin-dependent protein kinase II and its endogenous substrates in the induction of long-term potentiation. J Biol Chem 270:6119–6124
Gardoni F et al (1998) Calcium/calmodulin-dependent protein kinase II is associated with NR2A/B subunits of NMDA receptor in postsynaptic densities. J Neurochem 71:1733–1741
Gartner J, Freidlin MI (1979) On the propagation of concentration waves in periodic and random media. Sov Math Dokl 20:1282–1286
Hanson PI, Meyer T, Stryer L, Schulman H (1994) Dual role of calmodulin in autophosphorylation of multifunctional CaM Kinase may underlie decoding of calcium signal. Neuron 12:943–956
Hudmon A, Schulman H (2002) Neuronal Ca^{2+}/calmodulin-dependent protein kinase II: the role of structure and autoregulation in cellular function. Annu Rev Biochem 71:473–510
Holmes EE, Lewis MA, Banks JE, Veit RR (1994) Partial differential equations in ecology: spatial interactions and population dynamics. Ecology 75:17–29
Kinezaki N, Kawasaki K, Takasu F, Shigesada N (2003) Modeling biological invasions into periodically fragmented environments. Theor Popul Biol 64:291–302
Kolmogorov A, Petrovsky I, Piscounoff N (1937) Étude de l'équation de la diffusion avec croissance de la quantité de matière et son application à un problème biologique. Mosc Univ Bull Math 1:1–25
Konur S, Rabinowitz D, Fenstermaker VL, Yuste R (2003) Systematic regulation of spine sizes and densities in pyramidal neurons. J. Neurobiol. 56:95–112
Lee S-JR, Escobedo-Lozoya Y, Szatmari EM, Yasuda R (2009) Activation of CaMKII in single dendritic spines during long-term potentiation. Nature 458:299–304
Leonard AS, Lim IA, Hemsworth DE, Horne MC, Hell JW (1999) Calcium/calmodulin-dependent protein kinase II is associated with the *N*-methyl-D-aspartate receptor. Proc Natl Acad Sci USA 96:3239–3244
Lisman J, Schulman H, Cline H (2002) The molecular basis of CaMKII function in synaptic and behavioural memory. Nat Rev Neurosci 3:175–190
Lledo PM et al (1995) Calcium/calmodulin-dependent kinase II and long-term potentiation enhance synaptic transmission by the same mechanism. Proc Natl Acad Sci USA 92:11175–11179
Lou LL, Lloyd SJ, Schulman H (1986) Activation of the multifunctional Ca^{2+}/calmodulin-dependent protein kinase by autophosphorylation: ATP modulates production of an autonomous enzyme. Proc Natl Acad Sci USA 83:9497–9501
Malenka RC, Bear MF (2004) LTP and LTD: an embarrassment of riches. Neuron 44:5–21
Malinow R, Schulman H, Tsien RW (1989) Inhibition of postsynaptic PKC or CaMKII blocks induction but not expression of LTP. Science 245:862–866
Mammen AL, Kameyama K, Roche KW, Huganir RL (1997) Phosphorylation of the α-amino-3-hydroxyl-5-methyl-isoxazole-4-proprionic acid receptor GluR1 subunit by calcium/calmodulin-dependent protein kinase II. J Biol Chem 272:32528–32533
Mendez V, Fort J, Rotstein HG, Fedotov S (2003) Speed of reaction–diffusion fronts in spatially heterogeneous media. Phys Rev E 68:041105
Meunier C, d'Incamps BL (2008) Extending cable theory to heterogeneous dendrites. Neural Comput 20:1732–1775
Meyer T, Shen K (2000) In and out of the postsynaptic region: signalling proteins on the move. Trends Cell Biol 10:238–244
Miller SG, Kenney MB (1986) Regulation of brain type II Ca^{2+}/calmodulin-dependent protein kinase by autophosphorylation: a Ca^{2+}-triggered molecular switch. Cell 44:861–870
Murray JD (1989) Mathematical biology. Springer, Berlin
Noble JV (1974) Geographic and temporal development of plagues. Nature 250:726–729

Otmakhov N, Griffith LC, Lisman JE (1997) Postsynaptic inhibitors of calcium/calmodulin-dependent protein kinase type II block induction but not maintenance of pairing-induced long-term potentiation. J Neurosci 17:5357–5365

Panja D (2004) Effects of fluctuations on propagating fronts. Phys Rep 393:87–174

Pettit DL, Perlman S, Malinow R (1994) Potentiated transmission and prevention of further LTP by increased CaMKII activity in postsynaptic hippocampal slice neurons. Science 266:1881–1885

Rich RC, Schulman H (1998) Substrate-directed function of calmodulin in autophosphorylation of Ca^{2+}/calmodulin-dependent protein kinase II. J Biol Chem 273:28424–28429

Rose J, Jin S-X, Craig AM (2009) Heterosynaptic molecular dynamics: locally induced propagating synaptic accumulation of CaM Kinase II. Neuron 61:351–358

Saitoh T, Schwartz JH (1985) Phosphorylation-dependent subcellular translocation of a Ca^{2+}/calmodulin-dependent protein kinase produces an autonomous enzyme in *Aplysia* neurons. J Cell Biol 100:835–842

Shen K, Tereul MN, Subramanian K, Meyer T (1998) CaMKIIβ functions as an F-actin targeting module that localizes CaMKIIα/β heterooligomers to dendritic spines. Neuron 21:593–606

Shen K, Meyer T (1999) Dynamic control of CaMKII translocation and localization in hippocampal neurons by NMDA receptor simulation. Science 284:162–166

Shen K, Teruel MN, Connor JH, Shenolikar S, Meyer T (2000) Molecular memory by reversible translocation of calcium/calmodulin-dependent protein kinase II. Nat Neurosci 3:881–886

Shigesada N, Kawasaki K (1997) Biological invasions: theory and practice. Oxford University Press, Oxford

Shigesada N, Kawasaki K, Teramoto E (1986) Traveling periodic waves in heterogeneous environments. Theor Popul Biol 30:143–160

Strack S, Choi S, Lovinger DM, Colbran RJ (1997) Translocation of autophosphorylated calcium/calmodulin-dependent protein kinase II to the postsynaptic density. J Biol Chem 272:13467–13470

Torquato S (2002) Random heterogeneous materials. Springer, New York

van Saarloos W (2003) Front propagation into unstable states. Phys Rep 386:29–222

Volpert V, Petrovskii S (2009) Reaction–diffusion waves in biology. Phys Life Rev 6:267–310

Weinberger HF (2002) On spreading speeds and traveling waves for growth and migration in a periodic habitat. J Math Biol 45:511–548

Xin J (2000) Front propagation in heterogeneous media. SIAM Rev 42:161–230

Yang E, Schulman H (1999) Structural examination of autoregulation of multifunctional calcium/calmodulin-dependent protein kinase II. J Biol Chem 274:26199–26208

Yuste R (2010) Dendritic spines. MIT Press, Cambridge

Zhang Y-P, Holbro N, Oertner TG (2008) Optical induction of plasticity at single synapses reveals input-specific accumulation of αCaMKII. Proc Natl Acad Sci USA 105:12039–12044